A contribution to *MRS Advances*:

Macro-scale patterning for hierarchically designed thinner Peltier sheets

Norifusa Satoh[1], Jin Kawakita[1], Junnosuke Murakami[2]

[1] National Institute for Materials Science (NIMS), Tsukuba, 305-0044, Japan.

[2] Sekisui Chemical Company, Limited, Osaka, 618-0021, Japan.

Correspondence to: Dr. Norifusa Satoh, SATOH.Norifusa@nims.go.jp

Abstract

The global warming trend has made the world realize the importance of cooling technologies. Peltier devices potentially save 10-times energy consumption compared to only air conditioners being used, because of their capability of directly cooling down human body. Yet, commercial Peltier devices are still heavy, solid, and small. To mass-produce lighter-weight larger-area thinner Peltier sheets via a roll-to-roll process, we have developed sticky thermoelectric materials, hierarchically designed at atomic scale, nano scale, and micro scale. However, thought thinner Peltier sheets enable to physically enhance the cooling heat flux capability further, they require higher current at the maximum operating point, which ruin their cooling performance due to Joule heating on electrodes. In this study, we researched the macro-scale patterning of sticky TE materials and electrodes and discovered a stripe pattern being 14~23% better than the traditional check pattern. The simpler pattern could benefit mass production.

Introduction

The climate change has caused deadly heatwave to 25-50% of humankind without indoor cooling system [1]. To save human lives and reduce 68% of greenhouse gas emission from cooling sector by 2050, the United Nations launched the Global Cooling Pledge on Dec. 5, 2023. In the pledge, over 60 countries committed to penetrate highly efficient air conditioners into the market. Though current best available air conditioners have energy efficiencies two-to-three times higher than ones globally purchased [2], the global energy demand for space cooling is also expected to more than double by 2050 [3]. The simple comparison between the capability of available technology and the future demand indicates a technological gap toward net zero emission by 2050.

As a potential filler for the technological gap, thermoelectrics (TEs) can be a great candidate. Peltier human cooling devices can save energy consumption 10-times more than only air conditioners being used, because direct cooling of human body, especially neck vessels towards the brain, reduces the risk of heat-related illness and uncomfortableness to inhibit the start and power of air conditioners [4]. TE materials can generate Peltier temperature difference $\Delta T_{\mathrm{Peltier}}$ responding to the inputted electricity and the material properties: the figure of merit $Z = \alpha^2/\rho\kappa$, where α is Seebeck coefficient, ρ is electrical resistivity, and κ is thermal conductivity [5]. These material properties are competing each other but well optimized for commercialization. The limitation of current Peltier devices can be their heaviness, solidity, and small area size.

To mass-produce lighter-weight larger-area thinner Peltier sheets via a roll-to-roll process without using electrically conductive adhesives, we have been developing sticky thermoelectric materials [6-10] (Fig. 1a). To meet complex requirements, we have adapted a hierarchical multi-component strategy turning element composition of TE particles for high Seebeck coefficient at atomic scale [8], controlling the surface of TE particles for small interfacial electrical resistance at nano scale [8], and minimizing thermal conductivity and absorbing mechanical bending stress by hybridizing organic solvent with TE particles [7] and adopting ultra-thin high performance foam at micro-scale [10]. Physically speaking, "the thinner, the better!" [9,10] because the thinner feature allows Peltier sheets to be more flexible and can be applied to various shapes of objects leading to better heat transfer efficiency and to also cover enlarged area size using the same amount of TE materials for a higher coverage. Besides, the maximum heat flux capability q_{max} improves as thinning the thickness of TE layer t, as follows [11,12]:

$$q_{\max} = \frac{1}{t}(0.5\alpha^2 T_C^2/\rho - \kappa \Delta T_{\text{Peltier}}) \qquad (1)$$

where T_C is the temperature of cool side, T_H is the temperature of hot side, and $\Delta T_{\text{Peltier}} = T_H - T_C$. Assuming the same amount usage of TE materials for a higher coverage, the rate of heat transfer $Sq_{\max}$ for the t-thick Peltier sheet, where S is area size, can be enhanced by n^2 times for the t/n-thick Peltier sheet in total (Figure 1b) [10].

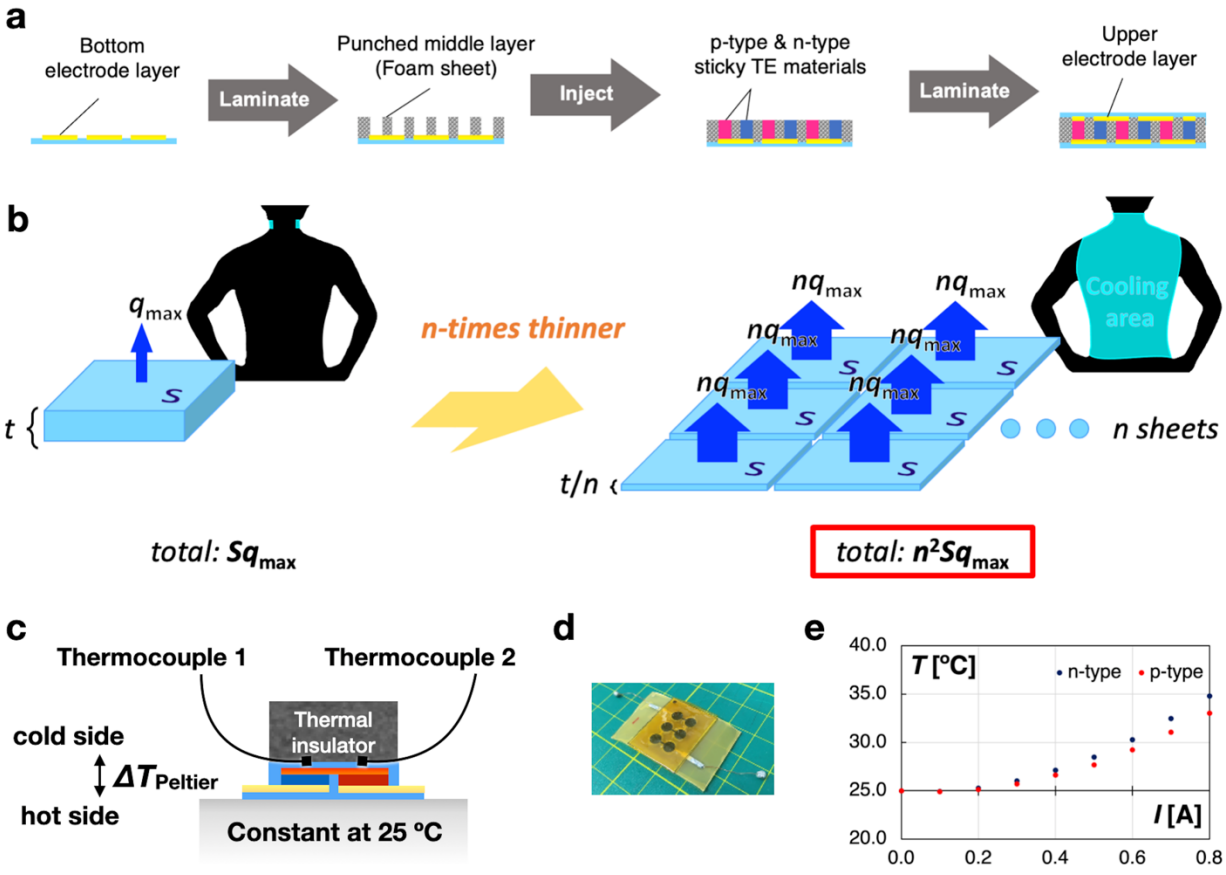

Fig. 1 **a** Scheme to fabricate the hierarchically-designed thinner Peltier sheets using the sticky TE materials. **b** Schematic comparison in the total $Sq_{\max}$ between a t-thick Peltier device and n sheets of t/n-thick Peltier sheets, using the same amount of TE material. **c** Characteristic of Peltier sheets under a temperature-controlled condition of the hot side. **d** Design of the previous pattern. **e** CP of the previous Peltier sheet.

Instead of the benefits on flexibility and the total Sq_{max}, Peltier sheets tend to ruin the cooling performance. The maximum temperature difference generatable inside TE materials ΔT_{max} is defined by their material properties, as follow: $\Delta T_{max} = 0.5ZT_C^2$ [5,11]. When achieving the ΔT_{max} for q_{max}, however, Peltier sheets require the following current density [11]:

$$i_q = \frac{1}{t} \cdot \alpha T_c / \rho \qquad (2)$$

Because thinner Peltier sheets require higher i_q, more Joule heat generates on electrodes. Under a free-standing condition of Peltier sheet, we have been able to observe the Peltier effect as the temperature difference between hot and cold sides because both side of the electrodes formed the almost same Joule heat [9,10]. To obtain the cooling effect from cold side, however, hot side is generally under a temperature-controlled condition (Fig. 1c). Because of the asymmetrical condition, Joule heating on the cold side critically matters to the cooling performance (CP). In the worst-case scenario, the previous Peltier sheets using narrow bridging electrodes optimized for TE generation [7] (Fig. 1d) demonstrate the Peltier effect under a free-standing condition [9] but no cooling effect under a temperature-controlled condition of $T_H = 25$ºC (Fig. 1e). The temperature of cold side simply increases with the applied current due to Joule heating. It means that Joule heating at the narrow bridging parts on the cold side conceals the potential CP based on the Peltier effect.

To design the macro-scale patterning of electrode and sticky TE materials, herein, we consider the heat generation rate per unit volume of electrode:

$$\frac{Q}{V} = \frac{1}{\sigma}\left(\frac{I}{A}\right)^2 \qquad (3)$$

$\because Q = RI^2$, $V = AL$, $R = L/\sigma A$, where Q is Joule heating per unit time, V is volume, σ is electrical conductivity of electrode, I is current, A is a cross-sectional area of electrode, R is resistance, L is length of electrode. When assuming the same width w for electrode and sticky TE materials' pattern to minimize Joule heating on the bridges, the w for $I \propto dw$ and $A = hw$ is canceled out each other in equation (3), where d is depth of sticky TE materials' pattern and h is height of electrode. It means that n-times shrinking of d, for example, reduces Q/V by n^2 times (Fig. 2). Comparing to the traditional check pattern of p-type and n-type TE materials in commercial Peltier devices, we can hypothesize that a stripe pattern with the same d benefits the CP of Peltier

sheets because of its small number of bridges required. In this study, we examine this hypothesis by comparing the single-π, stripe, and check patterns of the p-type and n-type sticky TE materials within the same area size.

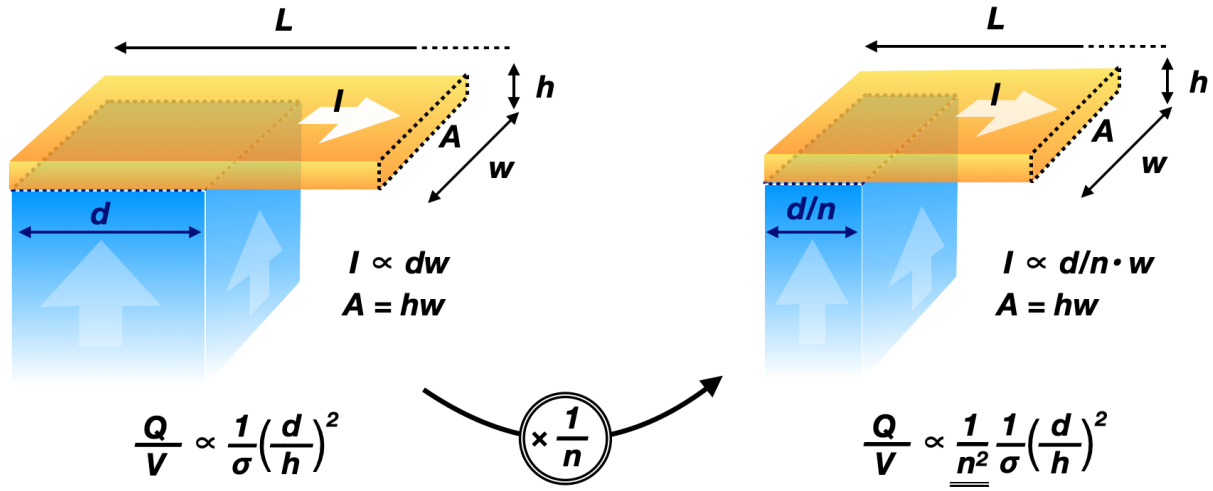

Fig. 2 Working hypothesis for the macro-scale patterning of Peltier sheets.

Experimental details

The sticky TE materials of partial Au skin Bi_2Te_3 particles of 150-300 μm were prepared as described in our previous paper [8]. To mix at the volume ratio of 50 %, the weight of Bi_2Te_3 particles was converted to the volume to calculate pipetting volume of palm shortening (trans-fat free, Daabon, Colombia) melted once at 60 ºC in a vacuum chamber for the purpose of vacuum drying. The upper and bottom electrode sheets (h = 18 μm) were fabricated as single-side flexible printed circuits (FPCs) by Scott Design System Co., Ltd., Japan. As the punched middle layer, the ultra-thin high performance foam (thickness: 0.3 mm, XLIM, Sekisui Chemical Co., Ltd., Japan) with double-coated adhesive were cut based on a programed pattern with a laser-cutting machine (VLS2.30DT, Universal Laser Systems, USA). After the underside of middle layers were sealed with the bottom electrode sheets, the hierarchically-designed sticky TE materials were injected into the patterned areas. The injection amount of sticky TE materials was defined based on the capsule volume calculated from the thickness of middle layers including two adhesive layers and the area of cut patterns. Finally, the deformable

sticky TE materials were sealed with the upper electrode sheets (Fig. 1a). Two power supply terminals (PV-4, MAC Eight Co., Ltd., Japan) were mounted on the surface of bottom electrodes for measurements.

To characterize the Peltier sheets based on the thermoelectric generation (TEG), the R and TE power V_{TE} were measured with a battery tester (BT3562A, Hioki E.E. Corporation, Japan), where the bottom side was cooled with an air-cooling Peltier plate (CHP-77HI, Sensor Controls Co., Ltd., Japan) at 20 ºC and the upper side was heated by a hot plate (PH200-100-PCC10A, MSA Factory Co., Ltd., Japan) at 40 ºC through a heat conductor. The applied temperature difference was 16 ºC, measured by two thermocouples (ST-11K-008-TS1-ASP, Anritsu Meter Co., Ltd., Japan) with a data logger (LR8432, Hioki E.E. Corporation, Japan). Note that the battery tester provides the equivalent data of TEG for that estimated from the I-V characteristics written in the previous paper [8].

To evaluate the CP, the Peltier sheets were placed on an air-cooling Peltier plate (CHP-77HI, Sensor Controls Co., Ltd., Japan) at 25 ºC and then the several different I was inputted with a DC Power Supply (PSW-360L30, ADC Corporation, Japan). The temperatures on the p-type and n-type upper electrodes (Fig. 1c) were measured with thermocouples (ST-11K-008-TS1-ASP, Anritsu Meter Co., Ltd., Japan) with a temperature input module (NI-9211, National Instruments Corp., USA) as the averages of 100-points stabilized data acquired at each 0.5 s under a program operation coded by Graphical Design Lab, Japan, based on LabVIEW 2017 (National Instruments Corp., USA).

Results and discussion

Table 1 summarizes a direct comparison of single-π, stripe, and check patterns in the design, TEG and CP. Each of the Peltier sheets presents the TEG as designed: the R increases linearly with the number of cells and inversely with the cell size and the V_{TE} also increases with the number of cells. Unlike the previous pattern (Fig. 1de), all the pattern in this research showed the negative CP thanks to the wide bridges. The best CP as the observed maximum $\Delta T_{Peltier}$ for the n-type and p-type cells, ΔT_n and ΔT_p, appeared in the stripe pattern, supporting the working hypothesis of the lowest Joule heating.

Herein, we can calculate the temperature increasing rate from the resistances and I at ΔT_p. The top electrode resistances for single-π, stripe, and check patterns can be estimated from the dimensions and $\sigma = 58.8 \times 10^6$ S/m to be 2.08 mΩ, 0.944 mΩ, and 2.38 mΩ, respectively. Using the volumes of top electrode, specific heat capacity 0.39 J/gºC, and density 890 kg/m^3 for Cu, the temperature increasing rate was calculated to be 3041 ºC/s, 2402 ºC/s, and 3753 ºC/s for the single-π, stripe, and check patterns, respectively. The calculation does not match the observed trend, especially for the relation of single-π and check patterns, because of ignoring heat dissipation from the heat-generating electrodes. The experimental results were obtained under a steady state of heat generation and dissipation.

Table 1 Comparison between single-π, stripe, and check patterns

Pattern		Single-π*1	Stripe*2	Check*3
Design	Upper	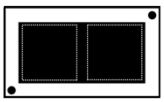	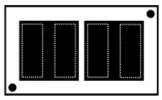	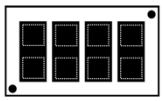
	Middle		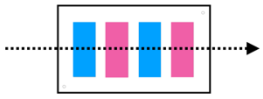	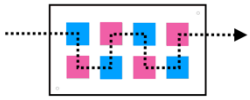
	Bottom	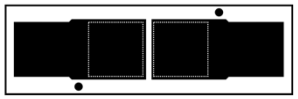	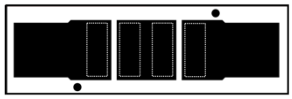	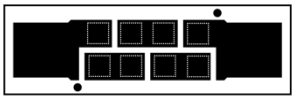
TEG	R (mΩ)	8.08	21.9	103
	V_{TE} (mV)	1.26	3.31	7.12
	$V_{TE}^2/4R$ (μW)	49.2	125	123
CP	Graph	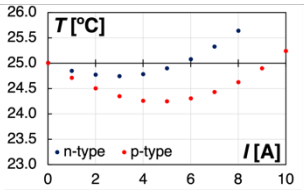	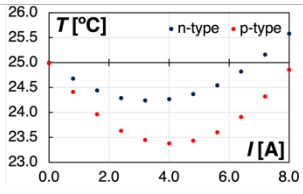	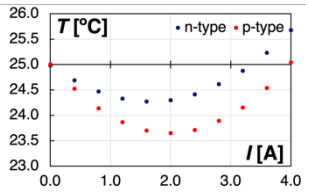
	ΔT_n (ºC)	0.3	0.8	0.7
	ΔT_p (ºC)	0.8	1.6	1.3

*1 dw = 10 mm × 10 mm, Line space: 2mm

*2 dw = 4 mm × 10 mm, Line space: 2mm

*3 dw = 4 mm × 4 mm, Line space: 2mm

To account for the difference between the patterns in ΔT_n and ΔT_p, we performed a one-dimensional steady-state heat conduction analysis (Table 2) [13]. Since the heat-generating top electrodes are connecting to the temperature-controlled plate of 25 ºC through the sticky TE materials at both sides (Fig. 1c), we can assume the problem as a one-dimensional heat conduction. Under the symmetrical boundary condition, the temperature distribution reaches the maximum T_0 at the midpoint of L. The temperature raised by Joule heating is discribed as follows:

$$T_{\text{raised}} = T_0 - 25 = \frac{\dot{q}}{2k}\left(\frac{L}{2}\right)^2 \qquad (4)$$

where $\dot{q} = Q/V$ shown as the equation (3), k is thermal conductivity of electrode. Based on a simpler one-dimensional model, yet the equation (4) includes the three-dimensional parameters of electrode, L and $A = hw$ to describe the difference between the patterns. In this analysis, the T_{raised} ordered the stripe, check, and finally single-π patterns from the smallest, which is coincident with the order observed in ΔT_n and ΔT_p resisting Joule heating of T_{raised}. Quantitatively and physically, the difference from the stripe pattern in T_{raised} is identical to the difference from the stripe pattern in ΔT_n or ΔT_p; abbreviated as calculated Δ^2 and observed Δ^2 in Table 2. The analysis supports the observed Δ^2 originates from the amount of Joule heating based on the electrode pattern as hypothesized.

Table 2 One-dimensional steady-state heat conduction analysis*1

Pattern	Single-π		Stripe		Check	
	n-type	p-type	n-type	p-type	n-type	p-type
I @ΔT_n or ΔT_p (A)	3	5	3.6	4	1.6	2
A (mm^2)	0.18	0.18	0.18	0.18	0.072	0.072
L (mm)	22	22	10	10	10	10
T_{raised} (ºC)	0.72	1.99	0.21	0.26	0.26	0.41
Calculated Δ^2 (ºC)	0.51	1.73	–	–	0.05	0.15
Observed Δ^2 (ºC)	0.5	0.8	–	–	0.1	0.3

*1 σ = 58.8 MS/m, k = 398 W/m·ºC

Finally, we estimate the cooling potential for p-type cell: $q = \kappa \Delta T_p / t'$, where t' is the total thickness of Peltier sheets. Because of $t' = 0.55$ mm for the stripe-pattern Peltier sheet, $q = 582$ W/m^2 based on the assumption of $\kappa = 0.2$ W/m^{o}C [7]. The value is larger than the metabolic rate 150 W/m^2 during walking/cycling and 250 W/m^2 during playing ball games [14]. Therefore, the Peltier sheets are highly potential to cool down a human body.

Conclusion

We have proposed stripe-patterned Peltier sheets that could benefit mass production thanks to their simpler design with 14~23% better performance than the traditional check-patterned sheets. Still, the sticky TE materials have room to improve the Z, especially ρ, by approximately two orders of magnitude [8]. Considering the Peltier sheets as a composite material hierarchically designed from atomic scale to macro scale including electrodes, we may be able to unlock a new possibility in TEs.

References

1. International Energy Agency. Sustainable, Affordable Cooling Can Save Tens of Thousands of Lives Each Year. (March 2023), https://www.iea.org/reports/sustainable-affordable-cooling-can-save-tens-of-thousands-of-lives-each-year. Accessed 3 June 2024
2. United Nations Environment Programme. Global Cooling Pledge for COP28. (December 2023), https://wedocs.unep.org/bitstream/handle/20.500.11822/44310/Global-Cooling-Pledge-final_231206_145613.pdf Accessed 3 June 2024
3. International Energy Agency. Net Zero Roadmap: A Global Pathway to Keep the 1.5 °C Goal in Reach. (September 2023), https://iea.blob.core.windows.net/assets/9a698da4-4002-4e53-8ef3-631d8971bf84/NetZeroRoadmap_AGlobalPathwaytoKeepthe1.5CGoalinReach-2023Update.pdf. Accessed 3 June 2024

4. K. Itao, H. Hosaka, K. Kiiaka, M. Takahashi, G. Lopes, Wearable equipment development for individually adaptive temperature-conditioning. J. Jpn. Soc. Precis. Eng. **82**, 919-924 (2016)
5. J. Mao, G. Chen, Z. Ren, Thermoelectric cooling materials. Nat. Matter. **20**, 454–461 (2020)
6. N. Satoh, M. Otsuka, T. Ohki, A. Ohi, Y. Sakurai, Y. Yamashita, T. Mori, Organic π-type thermoelectric module supported by photolithographic mold: a working hypothesis of sticky thermoelectric materials. Sci. Technol. Adv. Mater. **19**, 517–525 (2018)
7. N. Satoh, M. Otsuka, Y. Sakurai, T. Asami, Y. Goto, T. Kawamori, T. Masaki, G. Yatabe, J. Kawakita, T. Mori, Sticky thermoelectric materials for flexible thermoelectric modules to capture low–temperature waste heat. MRS Adv. **5**, 481–487 (2020)
8. N. Satoh, M. Otsuka, J. Kawakita, T. Mori, A hierarchical design for thermoelectric hybrid materials: Bi_2Te_3 particles covered by partial Au skins enhance thermoelectric performance in sticky thermoelectric materials. Soft Sci. **2**, 15 (2022)
9. N. Satoh, M. Otsuka, J. Kawakita, Hierarchically designed sticky thermoelectric materials to fabricate thinner Peltier sheets and device architectures. MRS Adv. **8**, 446–450 (2023)
10. N. Satoh, J. Kawakita, J. Murakami, J. Nakadate, T. Nakanishi, Sticky thermoelectric materials collaborate with ultra-thin high performance foam for hierarchically designed flexible Peltier sheets. MRS Adv. **8**, 781–786 (2023)
11. H. J. Goldsmid, in CRC Handbook of Thermoelectrics. ed. by D. M. Rowe (CRC Press, Boca Raton, 1995), pp. 19–26
12. I. Chowdhury, R. Prasher, K. Lofgreen, G. Chrysler, S. Narasimhan, R. Mahajan, D. Koester, R. Alley, R. Venkatasubramanian, On-chip cooling by superlattice-based thin-film thermoelectrics. Nat. Nanotechnol. **4**, 235–238 (2009)
13. T. Bergman, A. S. Lavine, F. P. Incropera, D. P. DeWitt, Introduction to Heat Transfer, 6th edition. (John Willey & Sons, Inc., Hoboken, 2011) pp. 142–145
14. A. Yorimoto, Physiological evaluation of WBGT index during exercise in heat. Jpn. J. Phys. Fitness Sports Med. **41**, 477–484 (1992)

Acknowledgment

The authors would like to thank Misaki Itakura for her technical assistance.

Funding

This study was funded by New Energy and Industrial Technology Development Organization (NEDO), JPNP20004, Norifusa SATOH.

Data availability

The data generated during the current study are available from the corresponding author on reasonable request.

Conflict of Interest

On behalf of all authors, the corresponding author states that there is no conflict of interest.

Author contributions

Norifusa Satoh designed the study concept, defined the experimental procedure, and analyzed the data to write the first draft of the manuscript based on the discussion with all authors. Junnosuke Murakami selected the appropriate foam sheet for this study and provided the handing instruction. All authors commented on the first draft to approve the manuscript.